Intuitive LTI energy-maximising control for multi-degree of freedom wave energy converters: The PeWEC case

Intuitive LTI energy-maximising control design for wave energy converters: the PEWEC case

Fabio Carapellese[a,*], Edoardo Pasta[a], Bruno Paduano[a], Nicolás Faedo[a], Giuliana Mattiazzo[a]

[a]*Marine Offshore Renewable Energy Lab., Department of Mechanical and Aerospace Engineering, Politecnico di Torino, 10129 Torino, Italy*

Abstract

Energy-maximising wave energy conversion control strategies are commonly based upon direct optimal control theory, where the control problem is discretised and transcribed into a nonlinear program, and a solution is found via numerical routines. Though appealing from an optimality viewpoint, the *real-time* application of such strategies to realistic (complex) wave energy systems, such as the PeWEC device, can become potentially challenging, due to its intrinsic multiple degree-of-freedom (DoF) nature. Furthermore, this pendulum-based system is not only multi-DoF in its nature, but also *underactuated*, *i.e.* only one mode, associated to the pendulum mechanism installed inside the wave-excited floating body, can be effectively actuated. We propose, in this paper, a set of four *simple and intuitive* energy-maximising controllers for the PeWEC system based, upon linear time-invariant (LTI) systems. We achieve this by deriving the so-called *impedance-matching* conditions for the PeWEC, and extending well-established LTI controllers, originally designed for fully actuated single-DoF systems, to this multi-DoF un-

*Corresponding author - E-mail: *fabio.carapellese@polito.it*

deractuated case. In particular, we explore, design, and synthesise both feedback, and feedforward configurations, making explicit emphasis in their main characteristics. Furthermore, we provide a performance assessment for each of the proposed controllers, showing their energy-maximising capabilities for the wave resource characterising the Mediterranean Sea.

---

1. Introduction

With more than 2 TW of resource power available worldwide, wave energy is one of the most promising renewable energy sources [19]. Since the '70s, researchers from a wide variety of backgrounds have been studying efficient ways to extract and store the energy generated by ocean waves [39, 40]. Independently from their design, wave energy converters (WECs) necessitate appropriate control technology to guarantee maximum energy extraction from the wave resource. The control algorithm that regulates the power take-off (PTO) system plays a fundamental role in maximising the extracted power, and hence in reducing the associated levelised cost of energy (LCoE). As such, efficient controllers are essential towards successful commercialisation of wide-spread WEC technology [38].

With the advancement of theoretical and applied research in modelling and control of wave energy extraction devices, several WEC systems, virtually always described and designed as multiple degree-of-freedom (DoF) devices, have been developed and tested over recent years (see *e.g.* [3, 17, 37, 49]). Moreover, not only such WECs are generally designed to operate in a multi-DoF fashion, but are naturally *underactuated*: Energy from incoming waves is often extracted only from a subset of its DoFs, typically happening

only *over a single mode of motion*, *e.g.* heave or pitch. This, almost inevitably, complicates the direct application/extrapolation of well-established control technology, originally developed for single DoF fully actuated WEC systems. A particular device, presenting such multi-DoF underactuated nature, is the so-called Pendulum Wave Energy Converter (PeWEC) [35], which is effectively the main concern of our study.

The PeWEC is a self-referenced inertial-based floating WEC which harvests the wave-induced motion on the floater to activate a resonant pendulum connected to an electric generator. As discussed in the previous paragraph, the PeWEC is inherently a multi-DoF underactuated WEC system, with its power-harvesting DoF being completely different from the wave-excited multiple modes of motion. These structural and dynamical qualities pose a challenge when attempting at applying well-known control algorithms to such a system, as further discussed in the following paragraphs.

Control system design for wave energy systems can be solved in terms of optimal control theory, where the control objective is, naturally, energy-maximisation. The vast majority of the optimal WEC control solutions available are based upon so-called direct optimal control theory (see *e.g.* [51]), where state, input, and objective variables are discretised accordingly. Alternatively, and depending on the nature of the model used to describe the associated WEC dynamics, such a control design procedure can be potentially solved in closed-form applying tools from calculus of variations [23]. For instance, [36] derives a optimal control law in the (closed) form of a static damping coefficient, derived via a deterministic approach. Another potential pathway is considered in [41], where a linear quadratic Gaussian (LQG)

controller is applied to an underactuated multi-tethered point absorber, and a full state-feedback control law is derived considering the stochastic nature of the corresponding wave excitation force.

Direct optimal control inherently requires numerical optimisation routines to solve for the resulting nonlinear program, such as in the case of model predictive control (MPC), and MPC-like controllers (see [9]). In particular, MPC has been widely considered in the process of solving the OCP associated with underactuated multi-DoF devices, as presented in, for instance, [42]. There are, although, at least two main disadvantages behind this family of controllers: convergence towards a globally optimal solution, and computational complexity of the resulting nonlinear optimisation program, are highly dependent upon the definition of the WEC model [6]. Since relatively 'large' (in terms of order) mathematical representations, *i.e.* models, are often required to accurately describe the motion of inherently multi-DoF systems, the real-time application of direct optimal control routines can be often unfeasible, hence hindering the practical value behind this set of strategies. An interesting alternative has been presented in [29], where a deep neural network (DNN) is trained to mimic an energy-maximising MPC (simulated offline), to overcome the potentially high computational costs. Despite [29] shows promising results in simulation for a particular WEC system, the method does not yet offer a formal closed-loop stability result, hence being difficult to guarantee performance specifications when applied to a different device.

Alternatives to direct optimal control techniques, which do not rely on potentially complex optimisation methods, have been also presented within

the WEC literature (see *e.g.* [13]). Such *simple* and *intuitive* controllers are fully based upon linear time-invariant (LTI) theory, avoiding the necessity of computationally demanding numerical optimisation routines. This family of simple controllers attempts to realise the anti-causal impedance-matching (IM) condition for maximum power transfer, by proposing classical control architectures [13]. Though particularly appealing within the WEC control community for its simplicity and degree of intuition when it comes to design and synthesis, such techniques are virtually always developed for single-DoF (and hence fully actuated) WEC devices, hindering its application for realistic multi-DoF underactuated devices, such as PeWEC.

Motivated by the simplicity and inherent appeal characterising IM-based control solutions, the main objective of this paper is to extend, design, and apply well-known LTI energy-maximising control strategies, originally developed for fully actuated systems, to the multi-DoF underactuated PeWEC device, based upon recent advances in IM theory for such a class of systems [8]. Then we develop *four simple and intuitive* controllers, characterised by well-known control architectures based upon fully LTI systems, for the PeWEC converter. In particular, both feedback and feedforward control architectures have been considered, assessing their performance in terms of energy absorption, while stressing their fundamental differences, and any limitations arising in their design and synthesis due to the multi-DoF underactuated nature of the system. The proposed methods are not only simple to design and synthesis, but have almost negligible computational requirements, and hence their implementation can be performed in real-time in virtually any hardware platform, being specially suitable for practical applications.

The reminder of this paper is organised as follows. Section 1.1 introduces any non-standard notation utilised in our study. Section 2 presents the PeWEC device and its associated control-oriented model. Section 3 derives and discusses the IM conditions for the underactuated multi-DoF PeWEC device, while Section 4 introduces the set of intuitive controllers proposed, organised according to its architecture (*i.e.* feedback and feedforward). Section 5 presents a performance assessment in terms of extracted power for each of the proposed control strategies, both in resonant and non-resonant conditions. Finally, Section 6 encompasses the main conclusions of our manuscript.

1.1. Notation

Standard notation is used throughout our paper, with any exception detailed in this section. $\mathbb{R}^+$ denotes the set of non-negative (non-positive) real numbers, while $\mathbb{C}_{<0}$ denotes the set of complex numbers with negative real-part. The symbol 0 stands for any zero element, dimensioned according to the context. The notation $\mathbb{N}_q$ indicates the set of all positive natural numbers up to q, *i.e.* $\mathbb{N}_q = \{1, 2, \ldots, q\}$. The *real-* and *imaginary-part* of a complex matrix $z \in \mathbb{C}^{n\times n}$ are denoted as $\Re(z)$ and $\Im(z)$, respectively. The Laplace transform of a function f (provided it exists), is denoted as $F(s)$, $s \in \mathbb{C}$. With some abuse of notation[1], the same is used for the Fourier transform of f, written as $F(\omega)$, with $\omega \in \mathbb{R}$. The *Hermitian* operator is denoted by $F^\star(\omega)$. The same notation is used for the analytic continuation of the Hermitian operator to the Laplace domain, *i.e.* the *parahermitian* conjugate,

[1]The use of the capitalised letter for Laplace and Fourier transforms is always clear from the context.

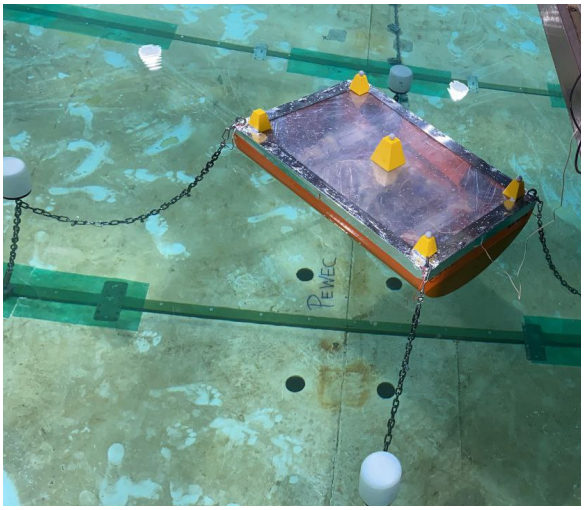

Figure 1: Picture of the 1:20 PeWEC prototype moored in a wave tank.

which is defined as $F^\star(s) = F(-s)^\intercal$, for $s \in \mathbb{C}$. In addition, we denote the Hermitian-inverse composition $F^{-1\star} = F^{\star-1}$ simply as $F^{-\star}$. Given a matrix $M \in \mathbb{C}^{n\times m}$, we denote its ij-th entry as M_{ij}, with $i \in \mathbb{N}_n$ and $j \in \mathbb{N}_m$. Likewise, given a vector $V \in \mathbb{R}^n$, we denote its i-th entry simply as V_i, with $i \in \mathbb{N}_n$.

2. PeWEC modelling

This section introduces the PeWEC, acronym of *pendulum wave energy converter*, an inertial self-referenced device composed of a pendulum system connected to the power take-off (PTO) mounted in a floating body. We can refer to Figure 1, where a 1:20 PeWEC prototype moored in wave tank is shown. The pitching motion of the floater δ induces a swinging motion ε of the pendulum, as described in Figure 2. The energy extraction from the system is achieved by damping the harmonic motion of the pendulum. A slack catenary type of 3-line mooring system, each line composed of a jumper

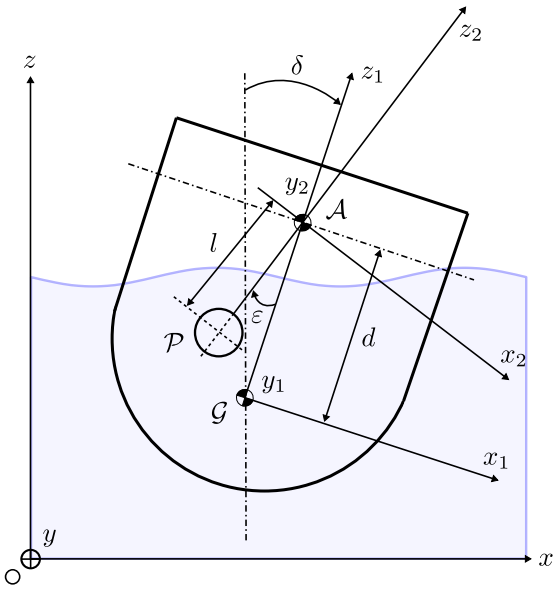

Figure 2: Schematic representation of the PeWEC device.

and a clump-weight, anchors the device to the seabed. The mooring system is designed to guarantee weather-vaning since the PeWEC device should always be orientated towards the incident wave [44, 27, 28]. Therefore, the vertical axis and the hull bow-stern direction define the wave-floater interaction on the plane. The PeWEC transfers the wave power to the pendulum, harvesting the hull-induced dynamics. In particular, the wave induces a motion on the hull body (expressed in the $Gx_1y_1z_1$ frame), generating a pendulum motion through the hinge defined in the $Gx_2y_2z_2$ frame. The mechanical power is then converted into electric power by an equivalent damping action exerted by the permanent magnet generator.

The pendulum equation of motion is dependent on the pose of the hull, referred to the inertial frame $Oxyz$, and its associated set of first and second derivatives. Let $p(t) = [x(t)\ z(t)\ \delta(t)]^T$, $p : \mathbb{R}^+ \to \mathbb{R}^3$, be the vector describ-

ing the position and orientation of the hull reference system $Ox_1y_1z_1$. Note that, in addition, there is a fourth DoF, describing the relative pendulum motion concerning the floater, being connected to the PTO axis. As such, one can now define the 'augmented' vector $q(t) = [p(t)\ \varepsilon(t)]^T$, $q : \mathbb{R}^+ \to \mathbb{R}^4$.

2.1. Linear model

We recall, in this section, the fundamental mathematical model describing the dynamics of the PeWEC device. In particular, we derive a linear model describing the behaviour of the WEC system about the equilibrium position, adopting a Lagrangian approach. Note that the models presented in this Section have been experimentally validated in [34, 35].

Remark 1. While the PeWEC system can be potentially described in terms of a nonlinear dynamical equation, *e.g.* when a hydraulic PTO system is considered as conversion mechanism (see [15]), such a case is beyond the scope of this study, which aims at developing simple and intuitive controllers for this WEC device, based upon linear time-invariant impedance-matching theory. As such, this section focuses on deriving a representative linear model, subsequently used in Section 3 to derive the corresponding energy-maximising IM conditions for control design and synthesis.

The PeWEC dynamical system can be hence formally introduced as[2]

$$M_p\ddot{q} + K_p q = f_{ex}, \tag{1}$$

where the matrices $M_p \in \mathbb{R}^{4\times4}$ and $K_p \in \mathbb{R}^{4\times4}$ define the coupling between the pendulum and the hull, providing the mathematical representation of the inertial reactions and restoring force due to the interaction between bodies. Moreover $f_{ex} : \mathbb{R}^+ \to \mathbb{R}^3$, $t \mapsto f_{ex}(t)$, is the total external force acting on the system. The angular displacement of both the floater and the pendulum

[2]From now on, the dependence on t is dropped when clear from the context.

are assumed to be zero at the origin of (1), and hence the linearised system matrices are defined as follows:

$$M_p = \begin{bmatrix} m_{\mathrm{TOT}} & & & * \\ 0 & m_{\mathrm{TOT}} & & \\ m_p(d-l) & 0 & I_y + I_p + I_b + m_p(d-l)^2 & \\ -m_p l & 0 & I_{p,A} - m_p dl & I_{p,A} \end{bmatrix},$$
$$K_p = \begin{bmatrix} 0\,0 & 0 & 0 \\ 0\,0 & 0 & 0 \\ 0\,0 & -gm_p(d-l) & gm_p l \\ 0\,0 & gm_p l & gm_p l \end{bmatrix}, \tag{2}$$

where $M_p = M_p^T$, $I_{p,A} = I_p + m_p l^2$, $m_{\mathrm{TOT}} = M + m_p + m_b$, M is the mass of the hull, I_y is the hull moment of inertia, g is the acceleration due to gravity, d is the distance between the device centre of gravity (CoG) and the pendulum fulcrum, l is the pendulum length, m_p and m_b define the pendulum mass and the support structure mass, respectively, and I_p and I_b are their associated moments of inertia. Finally, the so-called excitation vector F_{ex} is defined as

$$f_{ex}(t) = \begin{bmatrix} 0 & 0 & 0 & u(t) \end{bmatrix}^T, \tag{3}$$

where $u(t) \in \mathbb{R}$ is the control law, which is to be designed such as maximum energy absorption is achieved.

2.2. Hydrodynamics

In this section, the hydrodynamics of the PeWEC system, and its relevant equations, are presented. We recall that the floater is not *directly* involved

in the wave energy conversion process, but in fact is the main driver which transfers the incoming wave power to the PTO DoF of the system. As such, it is relevant to introduce the so-called wave-hull interaction dynamics, in terms of a suitable mathematical model.

With the assumption that the fluid is inviscible and incompressible, and the fluid flow is irrotational, the so-called *linear potential flow theory* [11, 21] provides an approximation of the fluid-structure interaction through a time-domain system of Volterra integro-differential equations Σ, written, for $t \in \mathbb{R}^+$, as

$$\Sigma : \begin{cases} M_f \ddot{p} = f_w + f_h + f_r + f_p, \\ v = \dot{p}, \end{cases} \tag{4}$$

where $v : \mathbb{R}^+ \to \mathbb{R}^3$ is the floater pose derivative, which for planar motion coincides with the velocity vector of the body, $f_w : \mathbb{R}^+ \to \mathbb{R}^3$ defines the (uncontrollable) wave excitation force, $f_p : \mathbb{R}^+ \to \mathbb{R}^3$ refers to the pendulum reaction force on the floater (see equation (3)), $f_r : \mathbb{R}^+ \to \mathbb{R}^3$ is the radiation force, and $M_f \in \mathbb{R}^{3\times3}$ is the generalized mass matrix of the hull referred to the frame $Gx_1x_2x_3$. The static term $f_h : \mathbb{R}^+ \to \mathbb{R}^3$ describes the pressure distribution over the body wetted surface in undisturbed conditions, and hence the hydrostatic restoring force acting on the floater. Such a force is defined proportional to the device pose, and can be hence written as $f_h(t) = -S_h p(t)$, where $S_h \in \mathbb{R}^{3\times3}$ is the so-called hydrostatic stiffness matrix.

The radiation force is modelled using the well-known Cummins' equation [5]. In particular, the radiation force acting on the i-th degree-of-freedom,

can be defined as

$$f_{r_i}(t) = -\sum_{j=1}^{n} \left(m_{ij}^{\infty} \ddot{p}_j(t) + \int_0^t h_{r_{ij}}(t-\tau)\dot{p}_j(t)d\tau \right), \tag{5}$$

where the first term in the summation, proportional to the device acceleration, corresponds to an inertial increase due to the water displaced when the body moves, while the second term corresponds with the dissipative force, proportional to the body velocity. In particular, m_{ij}^{∞} represents the so-called added-mass at infinite frequency, given by the relation $m_{ij}^{\infty} = \lim_{\omega \to +\infty} A_{r_{ij}}(\omega)$, where $A_r(\omega)$ is the frequency-dependent added-mass coefficient. Moreover, $h_r(t) \in \mathbb{R}^{3\times 3}$ is the causal radiation impulse response function containing the memory effect of the fluid response.

Remark 2. The matrix $A_r(\omega)$, together with the so-called frequency-dependent radiation damping $B_r(\omega)$, are commonly evaluated via hydrodynamic codes based upon boundary element methods (BEMs), such as NEMOH [1] or WAMIT [32]. Note that such coefficients can be fully characterised in terms of h_r, *i.e.*

$$\begin{aligned} A_{r_{ij}}(\omega) &= m_{ij}^{\infty} - \frac{1}{\omega}\int_{\mathbb{R}^+} h_{r_{ij}}(t)\sin\omega t\, dt, \\ B_{r_{ij}}(\omega) &= \int_{\mathbb{R}^+} h_{r_{ij}}(t)\cos\omega t\, dt. \end{aligned} \tag{6}$$

2.3. Control-oriented modelling

In the light of the upcoming results, this section presents a control-oriented linear WEC model for the PeWEC device [11]. Note that such a structure is largely used for control design and synthesis in Sections 3 and 4. In particular, we present an input-output frequency-domain model for the PeWEC dynamics, focusing on the definition of an *intrinsic impedance*, in the spirit of electric equivalents commonly used within the field of electronic engineering. We begin by noting that the radiation frequency-response

mapping can be fully defined in terms of the Fourier transform of h_r, *i.e.*

$$H_{r_{ij}}(\omega) = B_{r_{ij}}(\omega) + \jmath\omega[A_{r_{ij}}(\omega) - m_{ij}^{\infty}]. \tag{7}$$

With the relation posed in (7), system (1) can be represented, in steady-state conditions, by an equivalent impedance mapping I, where the floater (hydrodynamic) DoFs are affected by an uncontrollable wave excitation force F_w, while the PTO-related DoF is only directly affected by the user-defined control action U. Finally, the equation of motion of the floater can be written, in the frequency-domain, as

$$I(\omega)Q(\omega) = \begin{bmatrix} I_p(\omega) & \bar{I}_p(\omega) \\ \bar{I}_\varepsilon(\omega) & I_\varepsilon(\omega) \end{bmatrix} \begin{bmatrix} V(\omega) \\ \Lambda(\omega) \end{bmatrix} = \begin{bmatrix} F_w(\omega) \\ U(\omega) \end{bmatrix}, \tag{8}$$

where the mappings $V : \mathbb{R} \to \mathbb{C}^3$ and $\Lambda : \mathbb{R} \to \mathbb{C}$ represent the Fourier transform of the floater velocity vector v, and the pendulum velocity λ, respectively. Moreover, $I_p : \mathbb{R} \to \mathbb{C}^{3\times3}$, $\omega \to I_p(\omega)$, is the impedance matrix of the WEC, comprising both any hydrodynamic coupling, as well as mechanical interactions. In particular, each entry of the matrix $I_p(\omega)$ can be defined as

$$I_{p_{ij}}(\omega) = B_{r_{ij}}(\omega) + \jmath\omega \left[A_{r_{ij}}(\omega) + M_{p_{ij}} - \frac{s_{h_{ij}} + K_{p_{ij}}}{\omega^2} \right]. \tag{9}$$

The effect of the pendulum motion over the floater dynamics can be defined by the following equation:

$$\bar{I}_{p_i}(\omega) = \jmath\omega \left[M_{p_{i4}} - \frac{K_{p_{i4}}}{\omega^2} \right], \tag{10}$$

where $\bar{I}_p(\omega) \in \mathbb{C}^3$ is the coupling impedance vector, defined such that $\bar{I}_\varepsilon(\omega) = \bar{I}_p(\omega)^T$, hence representing the effect of the floater motion on the pendulum

dynamics. Finally, $I_\varepsilon(\omega) \in \mathbb{C}$, defined as

$$I_\varepsilon(\omega) = \jmath\omega \left[I_{p,A} - \frac{g m_p l}{\omega^2} \right], \tag{11}$$

is the impedance of the pendulum, characterised by its inertia with respect to the rotation axis, and the corresponding stiffness term.

2.4. Device characteristics

Following the frequency-domain model presented in Section 2.3, we now introduce the specific characteristics of the PeWEC device considered in our manuscript, used to provide an explicit derivation and analysis of the IM principle for this particular WEC geometry. We note that the chosen device is optimum concerning the levelised cost of energy (LCoE) objective, and its characteristics have been determined by a tailored optimisation process, introduced and described in [45],[4].

In particular, the hull of the system is made out of standard naval carpentry steel, with a density of $\rho_f = 7800$ [kgm^{-3}]. Consequently, considering the walls of the floater as thin plates, the profile is extruded over the $x - y$ plane, resulting in a prismatic shape. In particular, as detailed in Figure 3, the device can be characterised according to the following set of parameters:

- R_{eq}: Semi-length of the floater.
- R_1: Radius of circumference C_1.
- H: Overall height of the hull.
- *Draft*: Draft of the hull.
- R_2: Radius of circumference C_2.

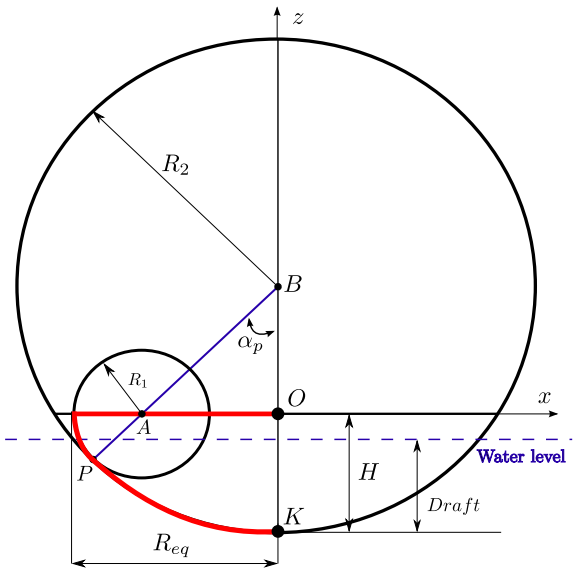

Figure 3: Parametric curve definition of the PeWEC profile on the $x - z$ plane.

- α_P: Tangency angle $\underline{/\text{PBO}}$.

Note that, as detailed in Figure 3, the hull profile is parameterised through simple curves. In particular, the bottom circumference, traced from point B, intersects the rim in the bow/stern section at the tangential point P. In contrast, the transversal section is constant for manufacturability and hydrodynamic advantages. Moreover, a subset of independent geometrical and inertial parameters can be defined as follows:

- W: Width of the floater.
- h: Bow/stern circumference ratio x_A/R.
- BFR: Ballast filling ratio, defined as the ratio of ballast located in the aft/fore ballast tanks over the total ballast[3].

[3]Note that a BFR = 1 indicates that all the ballast is stored in the aft/fore ballast

Table 1: Hull shape parameters.

Design Parameter	**Symbol**	**Units**	**Value**
Hull equivalent radius	R_{eq}	(m)	7.40
Hull width	W	(m)	22.5
Bow/stern circ. ratio	h	(-)	0.63
Tangency angle	α_p	(rad)	0
Radius of outer circ.	R_2	(m)	7.40
Height	H	(m)	7.40
Draft	$-$	(m)	4.81
Ballast filling ratio	BFR	(-)	0.54

We present, in Table 1, a full report of the parameters involved in the definition of the hull, as considered in this study. Note that, the solution found via optimisation (see [45] for further detail) brings to an even keel, parametrised with a single circumference that avoids a 'double curvature' solution. Finally, note that the ballast is equally distributed into the floater.

Continuing with the description of the device, Table 2 reports the set of parameters which define the inertial and geometric characteristics of the pendulum body. Each pendulum is composed of a cylinder parallel to the y-direction, swinging around a fulcrum. The volume of the cylinder is computed from its mass, considering the density of the steel. The mass is computed from the radius and height of the pendulum body that is controlled by the shape factor σ_p, which is a free design parameter[4]. Note that the relative

tanks, while BFR = 0 indicates that the totality of the ballast is stored in the bottom ballast tank)

[4]If the pendulum is *large and short*, then $\sigma_p = 0$, while if its defined to be *small and long*, then $\sigma_p = 10$.

Table 2: Pendulum characteristic parameters.

Design Parameter	**Symbol**	**Units**	**Value**
Number of pendulum/PTO	N_p	(-)	1
Pendulum mass	m_p	(ton)	7.17
Pendulum shape factor	σ_p	(-)	10
Pendulum arm length	l_p	(m)	2.40
Pendulum fulcrum	d	(m)	2.44

geometry of the hull and the pendulum allow for full rotation of the swinging mass around the fulcrum.

Given that the device has a single PTO system installed, the mounted pendulum is considerable large in terms of mass and dimension. Such a solution can bring advantages in terms of capital expenditure, since the cost related to the power conversion system drops considerably.

2.5. PeWEC operating conditions in the Mediterranean Sea

PeWEC is designed for the Mediterranean sea, a semi-enclosed sea with a medium wave energy power, characterised by a broadband energy distribution concentrated in a low-medium frequency range. According to [25] the Mediterranean Sea is less energetic than the oceanic sites but also presents less dangerous extreme conditions. The targeted installation site for the PeWEC is near Pantelleria island, in the Mediterranean Sea. Then according to Figure 4, the most representative waves for the PeWEC power assessment are characterised by an energetic period T_e that varies from 4 [s] to 8 [s], considering that the most occurrent waves have a significant height H_s of about 1 [m].

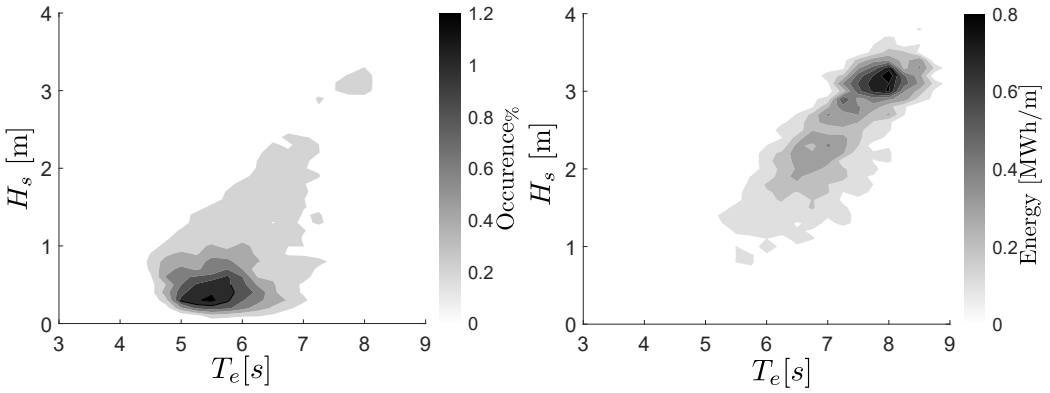

Figure 4: Occurrences (left) and energy (right) scatter diagrams for the reference site close to Pantelleria island, Italy.

3. Impedance-matching for PeWEC

Following the derivation presented in Section 2.3, the PeWEC dynamics can be fully represented by a multiple-input multiple-output (MIMO) transfer function $G_{sys}(s) \in \mathbb{C}^{4\times4}$. In particular, G_{sys} can be defined as the Laplace equivalent of I^{-1}, where I is the impedance matrix introduced in equation (8). Recall that each DoF associated with the floater dynamics is affected by an external uncontrollable wave excitation force input F_{w_i}, with $i \in \mathbb{N}_3$, but that energy is extracted by the pendulum *only in a single mode of motion*, which is controlled via a user-supplied control law u. The equation of motion describing such a controlled DoF (with velocity λ) can be fully written in Laplace-domain as

$$\Lambda(s) = G_\lambda(s)F_\lambda(s), \tag{12}$$

where $\{G_\lambda(s)^T, F_\lambda(s)\} \subset \mathbb{C}^4$, with[5]

$$G_\lambda^T = \begin{bmatrix} G_{sys_{41}} \\ G_{sys_{42}} \\ G_{sys_{43}} \\ G_{sys_{44}} \end{bmatrix} \begin{bmatrix} G_x \\ G_z \\ G_\delta \\ G_\varepsilon \end{bmatrix}, \quad F_\lambda = \begin{bmatrix} F_{w_1} \\ F_{w_2} \\ F_{w_3} \\ U \end{bmatrix} \begin{bmatrix} F_{w,x} \\ F_{w,z} \\ F_{w,\delta} \\ U \end{bmatrix}, \tag{13}$$

where each $G_{sys_j}(s) \in \mathbb{C}$, $j \in \mathbb{N}_4$, represents the mapping from the j-th input to the controlled output Λ. Note that, with the equivalent notation introduced in equation (13), the set $\{G_x(s), G_z(s), G_\delta(s)\}$ describes the floater-related dynamics affecting the output of the controlled DoF, while G_ε is the direct-link transfer function between the control action U, and the pendulum velocity Λ.

Remark 3. It is straightforward to show that the mapping G_ε, *i.e.* the transfer function characterising the map $u \mapsto \lambda$, is stable, minimum-phase, and positive-real. Furthermore, each element in the set $\{G_x(s), G_y(s), G_\delta(s)\}$ is stable. The interested reader is referred to, for instance, [48, 33], for further detail.

Figure 5 represents the Bode plot associated with G_ε. Note that the pendulum response is characterised by 'double peaks', *i.e.* multi-modal, given the inherent multi-DoF nature of the PeWEC system.

Remark 4. The transfer function $G_\varepsilon(s)$ for this particular PeWEC device, represented in Figure 5, is a strictly proper rational function of order 21, *i.e.* it has 21 (stable) poles and 20 (stable) zeros.

While the main pendulum dynamics, which are dependent on its geometrical and inertial properties, are 'located' in the high-frequency response of

[5]From now on, we drop the dependence on s when clear from the context, for simplicity of exposition.

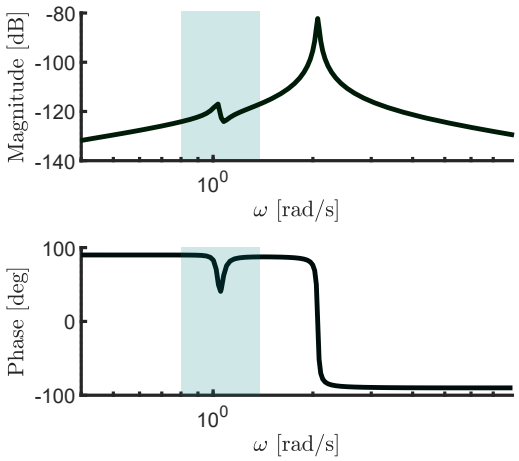

Figure 5: Bode plot of the pendulum mapping G_ε.

G_ε, the low frequency band is dominated by the floater dynamics. As such, two resonant conditions can be found, particularly when the forcing (input) frequencies are $\omega_1 = 1.05$ [rad/s] and $\omega_2 = 2.07$ [rad/s], where the first mode represents the hydrodynamic resonance, while the second mode is the natural frequency of the pendulum. In particular, note that the first mode of motion, contained within the shaded area depicted in Figure 5, represents the most relevant dynamics of the PeWEC from a control perspective, since it defines the behaviour of the WEC within its operating conditions, *i.e.* where the large part of the energy stored in the floater motion is effectively absorbed by the pendulum. This behaviour is referred to as *vibration quenching* [16].

Outside the shaded area indicated in Figure 5, the amplitude of the frequency-response of G_ε coincides with that of the stand-alone pendulum dynamics, *i.e.* the effect induced by the floater dynamics is minimal, and the swinging mass dynamics become dominant. Note that, in accordance with the design procedure, the floater geometry is defined, via global opti-

misation, to 'resonate' with the installation site's most characteristic power spectral density (PSD) functions, describing the wave resource. We recall that the PeWEC is designed for the Mediterranean sea, then the hydrodynamic resonance falls into the most energetic range of frequency, that for the Pantelleria site (see Section 2.5), corresponds to $\approx [0.9, 1.5]$ [rad/s]. Continuing with the dynamical description of the controlled DoF associated with PeWEC, and following the theory presented in [8], we note that equation (12) can be conveniently rewritten as

$$\Lambda = G_\varepsilon \left[\tilde{F}_w - U \right], \tag{14}$$

where the mapping $\tilde{F}_w$, defined as

$$\tilde{F}_w = \frac{G_x}{G_\varepsilon} F_{w,x} + \frac{G_z}{G_\varepsilon} F_{w,z} + \frac{G_\delta}{G_\varepsilon} F_{w,\delta}, \tag{15}$$

is the *total* wave excitation force acting on the controlled DoF, as schematically depicted in Figure 6.

Remark 5. The mapping $\tilde{F}_w$ is obtained by superimposing the contribution of each wave excitation force, acting on the corresponding floater DoFs, in the controlled output Λ. Note that such contributions are effectively modulated by an associated (stable) transfer function, *i.e.* G_x/G_ε, G_z/G_ε, and G_δ/G_ε, respectively.[6].

The derivations presented in (14)-(15) facilitate the definition of an intrinsic impedance for the controlled DoF: In particular, the impedance associated with the underactuated multi-DoF PeWEC system can be written [8] as

$$I_u = \frac{1}{G_\varepsilon}. \tag{16}$$

[6]The stability of $G_{sys_{ij}}/G_\varepsilon$, for all admissible pair (i, j), follows trivially from the minimum-phase property of G_ε (see Remark 3).

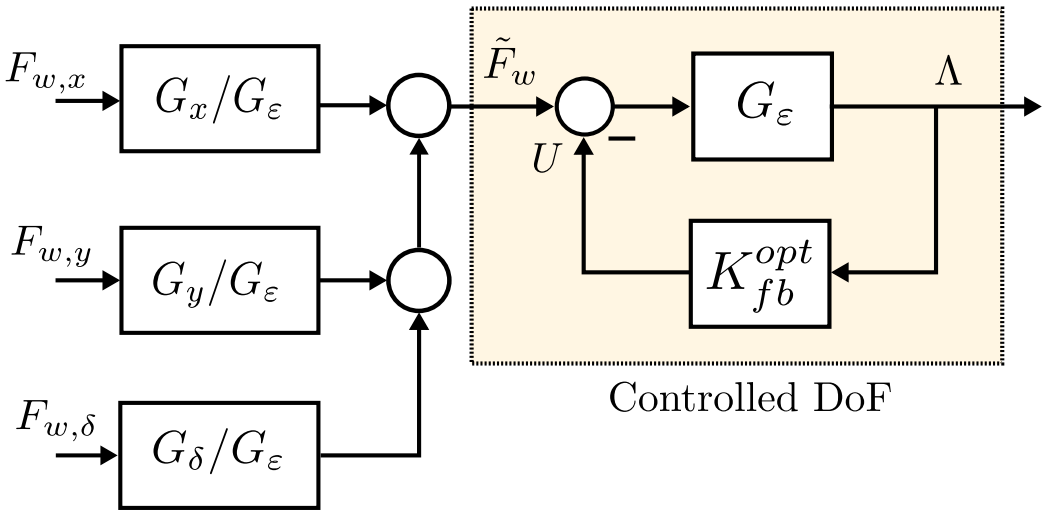

Figure 6: Impedance-matching-based feedback control-loop for the PeWEC device.

Applying the maximum power transfer (IM) theory, the optimal energy-maximising control force u can be then directly computed in terms of the parahermitian conjugate of G_ε (see [8]), *i.e.*

$$U = I_u^\star \Lambda = G_\varepsilon^{-\star} \Lambda = K_{fb}^{opt} \Lambda, \tag{17}$$

where the expression (17) directly highlights the feedback nature of the IM condition: The control action is defined by the 'modulation' of the output Λ by the anti-causal transfer function[7] K_{fb}^{opt}. The associated control-loop, with input $\tilde{F}_w$ (*i.e.* total wave excitation force), is depicted in Figure 6, while the frequency-response mapping characterising the optimal feedback controller K_{fb}^{opt} is depicted in Figure 7 (right).

In particular, the optimal control action in (17) is derived from the output velocity signal of the pendulum λ modulated by $G_u^{-\star}$ and, hence, the optimal

[7]The anti-causality of K_{fb}^{opt} is both linked to the relative degree of G_ε, and the nature of the parahermitian operator. The interested reader is referred to [8] for further detail.

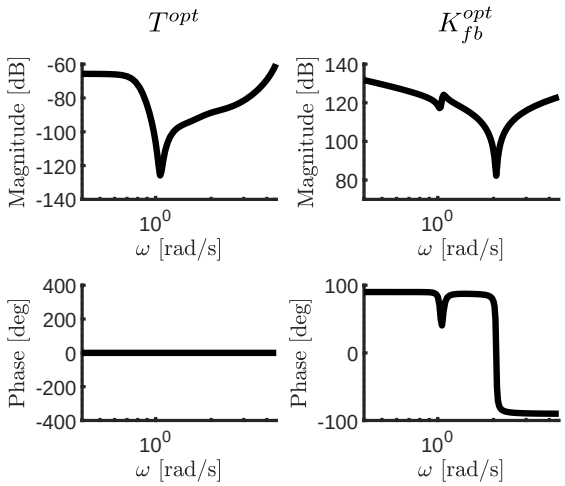

Figure 7: Optimal force-to-velocity frequency-response $T^{opt}(\omega)$ (left), along with the corresponding optimal feedback controller $K_{fb}^{opt}(\omega)$ (right).

closed-loop input-output response T^{opt}, characterising the *force-to-velocity* map $\tilde{F}_w \mapsto \Lambda$, under controlled conditions, is given by

$$T^{\text{opt}} = \frac{G_\varepsilon G_\varepsilon^\star}{G_\varepsilon + G_\varepsilon^\star}, \tag{18}$$

where, due to the properties of G_ε, it is straighforward to check that $T^{\text{opt}} : \mathbb{C} \to \mathbb{R}^+$, *i.e.* T^{opt} is an ideal zero-phase filter (see Figure 7 - left).

Remark 6. The optimal IM controller K_{fb}^{opt}, expressed in (17), and its associated closed-loop response (18), are impossible to implement directly in practice, due to the inherent anti-causality of $G^{-\star}$. Nonetheless, one can approximate such optimal behaviour via stable and causal (i.e. implementable) control structures via suitable methods (*e.g.* interpolation and/or system identification [24]), such as those proposed herein in Section 4.

Following Remark 6, we note that the frequency-response mapping characterising K_{fb}^{opt} in Figure 7 (right), directly highlights one fundamental challenge when attempting at designing energy maximising control techniques for the multi-DoF underactuated PeWEC device: The relevant dynamics (*i.e.*

those characterising the behaviour of the device for the frequency range associated with the wave resource) are somewhat 'hidden' by the pendulum dynamics, which become largely dominant in the overall system response. This naturally poses a challenge when attempting at computing an accurate approximation of such optimal control condition via *e.g.* standard LTI system identification procedures.

4. Control design procedure

In this section, we propose, design, and synthesise, a set of suitable energy-maximising controllers for the PeWEC device, operating in wave conditions characterising the Mediterranean sea. Recall that the optimal IM condition for PeWEC has been introduced in Section 3, highlighting that intrinsic non-causality behind the energy maximising control condition. Nonetheless, as detailed in Remark 6, stable and causal LTI structures can be used to approximate the optimality condition posed in equation (17), by means of, for instance, frequency-domain interpolation, or black-box system identification procedures (see [24]).

Motivated by this, we introduce, in this section, a set of *four simple and intuitive* controllers based upon LTI systems theory (hence having minimal computational requirements), to maximise energy extraction for the PeWEC converter, explicitly via the pendulum (controlled) DoF. In particular, we explore different control architectures, well-established in classic and modern control literature: Feedback and feedforward configurations, presented in Sections 4.1 and 4.2, respectively. The proposed controllers are explicitly designed to approximate the IM condition derived in equation (17), hence

directly attempting at maximising energy absorption. We make explicit emphasis in exposing the advantages and disadvantages characterising each type of control structure, highlighting, at the same time, the most crucial aspects regarding synthesis for each approach.

4.1. Feedback control architectures

Recall that, according to the IM condition derived in equation (17), the optimal power transfer can achieved via a velocity feedback controller K_{fb}^{opt}, defined in terms of the parahermitian conjugate of G_{ε}. As discussed in Section 3 (see also Remark 6), K_{fb}^{opt} cannot be physically implemented, and hence the optimal condition needs to be approximated in terms of a *stable and causal* controller K_{fb}. In particular any controller K_{fb} is to be defined such that the following condition

$$\left\| K_{fb}(\omega) - K_{fb}^{opt}(\omega) \right\|_2 \approx 0, \quad \omega \in \mathcal{W}, \tag{19}$$

holds, where $\mathcal{W} \subset \mathbb{R}$ defines a frequency range of interest (often directly related with the nature of the wave resource). We discuss three different synthesis procedures, listed in the upcoming sections.

Note that one main advantage of this family of feedback controllers is that only output measurements are required to implement the associated structure. This is in constrast to the set of feedforward controllers presented in Section 4.2, which inherently necessitate an estimate of any external (uncontrollable) forces (*i.e.* wave excitation forces). Nonetheless, as detailed throughout this section, feedback controllers are, in general, less convenient from a stability viewpoint if designed via (19): Even though one can compute a system K_{fb} minimising (19), there is, in general, no guarantee of a stable

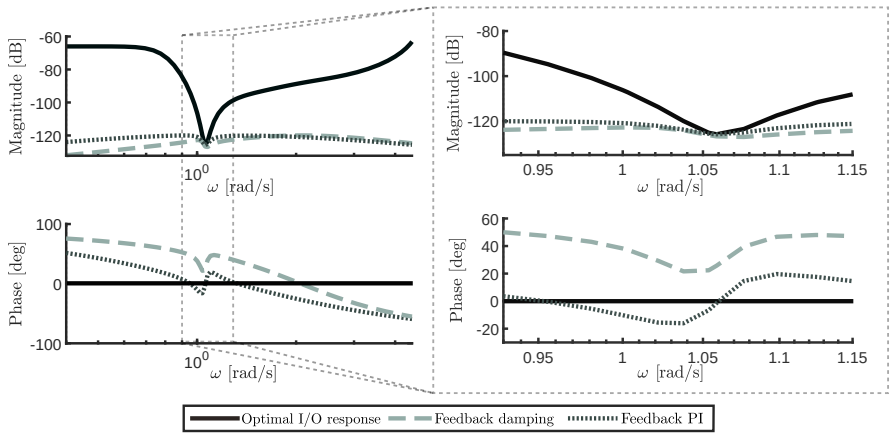

Figure 8: Closed-loop (I/O) frequency-response behaviour for the proposed set of feedback controllers.

closed-loop behaviour, *i.e.* the set of poles associated with the map

$$T_{fb} = \frac{G_\varepsilon}{1 + K_{fb} G_\varepsilon}, \tag{20}$$

is not necessarily contained in $\mathbb{C}_{<0}$. This, naturally, directly limits the parametric complexity that can be associated to K_{fb} when attemping at fulfilling (19) while rendering, at the same time, a stable closed-loop map T_{fb}.

4.1.1. Static damping (proportional) control

Being one of the most popular approaches in many single-DoF wave energy systems, this strategy is based upon an input of the damping type, *i.e.* by modelling the PTO as a (constant) viscous damper

$$K_{fb}^{opt} = k_p, \tag{21}$$

where $k_p \in \mathbb{R}^+$ is the static gain characterising the proportional controller. Note that such a controller can be generated simply by changing the magnetic field flux acting across the meshes of the electric generator, so it becomes almost straightforward to implement in practice. Following the criteria posed

in (19), we design the parameter k_p to fulfill the following interpolation condition:

$$K_{fb}(\omega_i) = k_p = \left|K_{fb}^{opt}(\omega_i)\right|, \tag{22}$$

where ω_i is a suitably defined interpolation frequency. For this case, ω_i is chosen as the frequency characterising the hydrodynamic resonance peak, *i.e.* $\omega_i = 1.05$ [rad/s]. The resulting closed-loop response T_{fb}, for the controller defined via (22), can be appreciated in the Bode plot of Figure 8 with a dashed-gray line. Note that the interpolation condition is effectively being respected, and the controller designed is such that the magnitude of the closed-loop behaviour interpolates the optimal T^{opt} for $\omega_i = 1.05$ [rad/s]. We highlight that closed-loop stability, for this particularly simple control structure, is always guaranteed: Since G_ε is stable and positive-real, and $k_p \in \mathbb{R}^+$, their feedback interconnection (as in equation (20)) is automatically stable (see *e.g.* [50]).

4.1.2. Proportional-integral (PI) control

This type of controller is also widespread within the wave energy community, both for single-DoF, and multi-DoF WEC devices. Nonetheless, when it comes to multi-DoF underactuated devices, PI controllers are often designed based upon potentially complex (and time consuming) optimisation routines [2, 47], aiming at numerically finding the associated set of optimal PI parameters to maximise energy extraction. In contrast to these approaches, we show herein that the derivation of the optimal condition (17) facilitates an immediate optimal design for such a PI structure. In particular, note that the PI controller generates a control action proportional to the angular

velocity λ, and the angular rotation ε of the pendulum, *i.e.*

$$K_{fb}(s) = k_p + \frac{k_i}{s}, \tag{23}$$

where k_p and k_i are selected to interpolate $K_{fb}^{opt}(\omega)$, as defined in (17), at a (suitably selected) frequency of $\omega_i = 1.05$ [rad/s] (see also the discussion provided in Section 4.1.1). Note that, due to the integral term in (23), this strategy is often referred to as *reactive control*, since the corresponding electric generator can potentially behave as a motor, resulting in a bi-directional power flow. In particular, it is straightforward to show that $K_{fb}(\omega_i) = K_{fb}^{opt}(\omega_i)$ if and only if

$$k_p = \Re\left\{K_{fb}^{opt}(\omega_i)\right\} \text{ and } k_i = -\omega_i \Im\left\{K_{fb}^{opt}(\omega_i)\right\}, \tag{24}$$

and hence the set of parameters characterising the optimal PI (23) can be computed without the need of any potentially complex optimisation routines, via equation (24).

The closed-loop response T_{fb} for the PeWEC device, arising from the controller (23), is shown in Figure 8, using a dotted-black line. Note that, as per design and synthesis, the corresponding PI controller interpolates *both amplitude and phase* of the optimal response $T^{opt}(\omega)$, at the desired interpolation frequency ω_i. We do highlight that the interpolation condition in (24) does not intrinsically guarantee closed-loop stability, in contrast to the case of the proportional controller described in Section 4.1.1. Nonetheless, for the particular case of PeWEC, and the chosen interpolation point ω_i, the associated closed-loop response T_{fb} is effectively stable.

4.2. Feedforward control architectures

In contrast with the feedback architecture introduced in Section 4.1, we now propose two different feedforward control structures. Such controllers are based upon 'transforming' the feedback condition in equation (17) into an equivalent feedforward calculation. Unlike the feedback schemes presented in Section 4.1, the overall stability of the control loop can be systematically (and straightforwardly guaranteed) via this set of feedforward controllers, hence facilitating the use of more sophisticated systems to approximate the energy-maximising optimality condition. Though highly convenient from a stability viewpoint, the actual implementation of these feedforward schemes inherently require an estimate of the external (uncontrollable) input affecting the PeWEC system, which is non-measurable in practice (see, for instance, [31]).

Nonetheless, a key feature, arising directly from the derivation of the IM condition for PeWEC in Section 3, is that the associated optimal control loop can be seen as an I/O system affected by the so-called *total* excitation force $\tilde{F}_w$ affecting the controlled (pendulum) DoF, expressed in equation (15). In other words, and unlike current WEC control literature for underactuated multi-DoF systems, which commonly estimate the 'full' wave excitation force vector F_w, the feedforward controllers proposed in this section only require an estimate $\hat{\tilde{F}}_w$ of $\tilde{F}_w$, *i.e.* the estimation problem is inherently SISO. This naturally simplifies the associated design process, hence being more intuitive and straightforward to implement in practice. A more detailed description of the specific estimation technique employed is presented in Section 4.2.3.

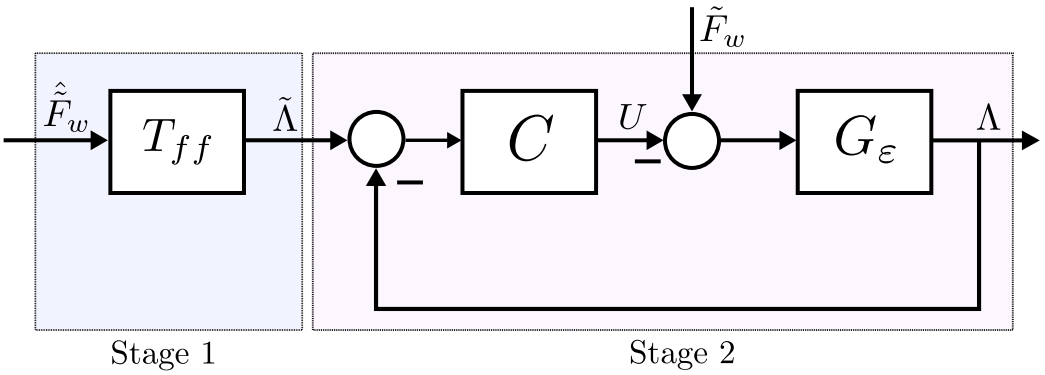

Figure 9: Schematic representation of the (multi-stage) feedforward constant control loop.

4.2.1. Feedforward constant

The feedforward controller presented in this section, termed *feedforward constant*, is inspired by the study presented in [12], and hence is based upon the determination of an optimal energy-maximising velocity profile $\tilde{\lambda}$ of the pendulum. This is effectively performed through the computation of a stable and causal transfer function which approximates the optimal closed-loop force-to-velocity mapping T^{opt} defined in (18), and a suitable estimate $\hat{\tilde{F}}_w$ of the total excitation force acting on the pendulum DoF (see Section 4.2.3). The general structure of this controller, which is shown in Figure 9, can be divided into two main blocks: Stage 1 and Stage 2.

Stage 1, which effectively deals with the generation of the corresponding optimal velocity profile, is based upon synthesising a *constant* filter T_{ff} fulfilling

$$T_{ff} = T^{opt}(\omega_i) \in \mathbb{R}^+, \tag{25}$$

for a given frequency point of $\omega_i = 1.05$ [rad/s] (in the same spirit as in Section 4.1). The Bode plot associated with the resulting controller is shown in Figure 10, using a dashed-grey line. Note that the optimal zero-phase

condition is naturally matched $\forall\omega$, given the constant nature of the filter.

Stage 2 concerns the design and synthesis of a feedback tracking controller C, capable of asymptotically track the computed optimal velocity profile, in spite of the presence of the external (uncontrollable) input $\tilde{F}_w$, *i.e.* the total excitation force acting on the controlled DoF. The controller C is here synthesised via the so-called Youla-Kŭcera approach (see, for instance, [18]), as detailed in the following. Let $Q_C : \mathbb{C} \to \mathbb{C}$, $s \mapsto Q_C(s)$ be a proper rational transfer function, and define the family of all stabilising controllers C parameterised in Q_C for the controlled DoF G_ε as

$$C = \frac{Q_C}{1 - Q_C G_\varepsilon}. \tag{26}$$

Given the minimum-phase property of G_ε (see Section 3), we can directly define Q_C in terms of the principle of plant inversion, *i.e.*

$$Q_C = F_C G_\varepsilon^{-1}, \tag{27}$$

with F_C the so-called *shaping filter*, designed to be stable, have relative degree such that (27) is proper, and accomplish the frequency-domain condition $F_C(\omega) \approx 1$ in the frequency range characterising the optimal reference input. The latter guarantees that the map $\tilde{\lambda} \mapsto \lambda$ is approximately an identity, and hence $\lambda \approx \tilde{\lambda}$ when $t \to +\infty$. The shaping filter F_C is herein selected in terms of a simple structure with multiple real poles placed at the same location in $\mathbb{C}$, *i.e.*

$$F_C(s) = \frac{1}{\left(\frac{1}{\omega_c}s + 1\right)^{n_Q}}, \tag{28}$$

where $\omega_c \in \mathbb{R}^+$ is the so-called *cutoff* point, which is set to $\omega_c = 30$ [rad/s], and n_Q is the multiplicity associated with the pole $s = \omega_c$, selected as $n_Q = 2$

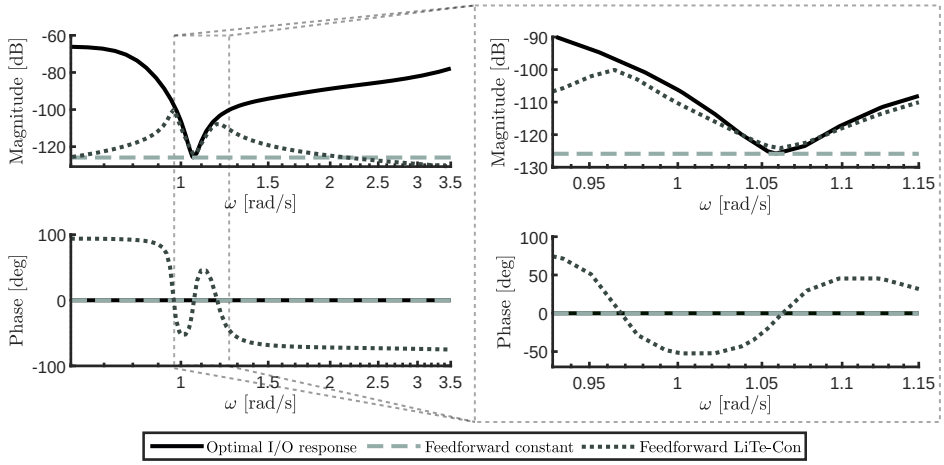

Figure 10: Closed-loop (I/O) frequency-response behaviour for the proposed set of feedback controllers.

(which is the minimum degree required to render (26) proper, and hence implementable).

4.2.2. Feedforward LiTe-Con

The LiTe-Con control structure, originally developed for single-DoF devices in [14], attempts at realising the IM principle in terms of a feedforward control injection, hence also relying upon an estimate $\hat{\tilde{F}}_w$ of the total wave excitation force acting on the controlled (pendulum) DoF (see Section 4.2.3). In particular, adapting and extending the results presented in [14], we can re-write the optimal condition (17), derived for the multi-DoF underactuated PeWEC system, in terms of an equivalent feedforward mapping

$$H_{ff}^{opt} = \frac{G_\varepsilon}{G_\varepsilon + G_\varepsilon^\star}, \tag{29}$$

which only depends upon G_ε. Due to the instrisic nature of equation (29), H_{ff}^{opt} is also non-causal (and hence impossible to implement directly), consistently with the non-causality of its analogous feedback condition (17). Based

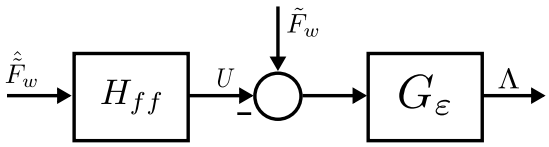

Figure 11: LiTe-Con-based feedforward controller architecture for PeWEC.

upon (29), we now make explicit use of black-box system identification routines (see *e.g.* [24]) to compute an approximating LTI stable and causal filter H_{ff} fulfilling

$$\left\| H_{ff}(\omega) - H_{ff}^{opt}(\omega) \right\|_2 \approx 0, \quad \omega \in \mathcal{W}, \tag{30}$$

where the set $\mathcal{W}$ is chosen as $\mathcal{W} = [0.9, 1.5]$ [rad/s], which corresponds with the spectral characterisation of the wave resource in the Mediterranean sea (see also Section 3). The resulting H_{ff} controller has been computed using moment-matching-based system identification procedures, as recalled in [10], and implemented via the software FOAMM [30], resulting in an LTI system of order 25.

A Bode plot of the computed filter can be appreciated in Figure 12 (solid-green), where the shaded area denotes the frequency range $\mathcal{W}$ considered for the corresponding identification process, showing a satisfactory approximation of the optimal condition (solid-black) for the set $\mathcal{W}$ (particularly in terms of magnitude). Furthermore, the associated closed-loop (I/O) response, *i.e.* $T_{ff} = H_{ff} G_\varepsilon$, can be appreciated in Figure 10 (dotted-black), together with that of the corresponding optimal map T^{opt} (solid-black), showing an agreement consistent with that in Figure 12.

4.2.3. Estimator design

As detailed throughout Section 4.2, both proposed feedforward configurations inherently require knowledge of the total wave excitation force $\tilde{F}_w$

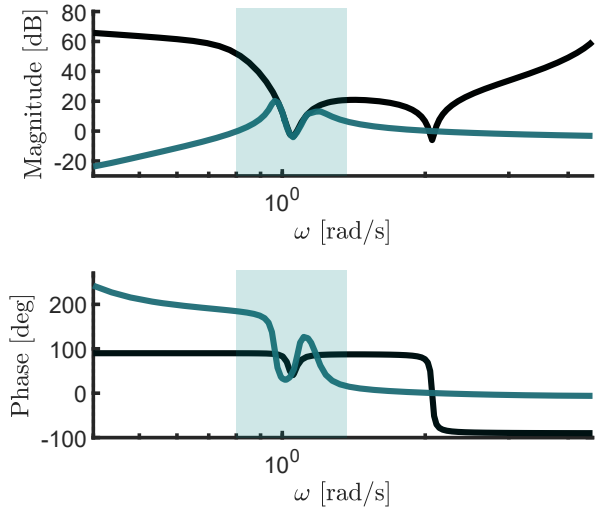

Figure 12: Bode plot of the optimal controller frequency response H_{ff} (solid-green), along with the frequency-response of the optimal feedforward IM condition H_{ff}^{opt}. The green area denotes the corresponding frequency range $\mathcal{W}$.

acting on the controlled DoF, which is not measurable in practice. To compute an estimate $\hat{\tilde{F}}_w$ of the unknown input, we consider the so-called *simple and effective* estimation technique presented in [7], which re-formulates the unknown-input estimation problem in terms of a (dual) control tracking loop. In particular, a Youla-Kŭcera parametrisation is considered (as in Section 4.2.1), where a tracking controller C is designed to achieve asymptotic tracking of the measured velocity of the pendulum DoF (see Figure 13). The associated Youla parameter Q_C is chosen as in (27), with the very same shaping filter (28). We refer the reader to [7] for an analysis of the stability and convergence of this technique under the assumptions posed in this study for G_ε.

Finally, and aiming to provide an example case concerning the performance of the designed estimator, Figure 14 shows the time-trace of a specific

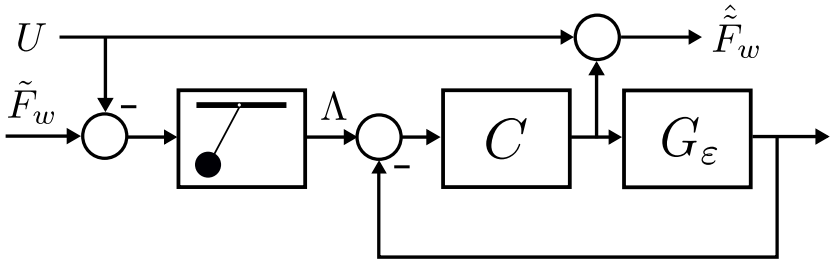

Figure 13: Schematic representation of the total wave excitation force estimator.

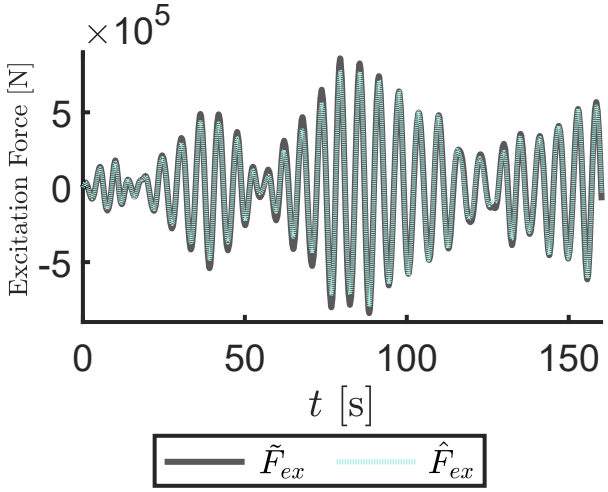

Figure 14: Time-trace of the actual pendulum excitation force $\tilde{F}_w$, generated with a typical sea state corresponding to the Mediterranean sea, and the estimated excitation force $\hat{\tilde{F}}_w$.

total wave excitation force[8] $\tilde{F}_w$ (solid-black), and the corresponding estimate $\hat{\tilde{F}}_w$ (dotted-gray), obtained via the synthesised estimator. It can be readily appreciated that both signals are virtually identical (up to graphical accuracy), hence highlighting the satisfactory performance of the designed estimator.

[8]The total wave excitation force used for Figure 14 has been generated stochastically, using a wave spectrum characterising the resource in the Mediterranean sea. The reader is referred to Section 5 for further detail.

Table 3: PTO system characteristics.

Design Parameter	**Symbol**	**Units**	**Value**
Maximum torque	T_{max}	(kNm)	40
Maximum speed	ω_{max}	(rad/s)	36
Nominal Torque	T_{nom}	(kNm)	20
Nominal speed	ω_{nom}	(rad/s)	26
Gear ratio	τ	-	30

5. Performance analysis

In this section, we analyse the control performance obtained for each of the controllers presented, designed, and sythesised in Section 4. In particular, the performance of each structure is evaluated in terms of electric power converted by the PeWEC PTO system, *i.e.* in terms of their energy-maximising capabilities. For the upcoming simulations, wave inputs are generated considering a JONSWAP spectral density function (SDF) [20] using a deterministic amplitude scheme (see [26]). In particular, according to a harmonic-superposition method, the corresponding spectrum is discretised in N frequencies $\omega_k = k\Delta\omega$, $k \in \mathbb{N}_N$, where $\Delta\omega = 2\pi/T_{sim}$, with T_{sim} the corresponding simulation time, set to $T_{sim} = 3600$ [s]. Note that T_{sim} is chosen to be sufficiently large so as to obtain statistically consistent results for the upcoming performance assessment. Furthermore, an explicit list of the parameters associated with the PTO system is offered in Table 3, so as to clarify the main characteristics of the chosen actuator. These will, naturally, have a direct impact on the actual implementation of any control solution.

To begin with the corresponding performance assessment, Figure 15 shows

produced power for each of the designed and synthesised control laws (see Section 4), for a randomly realised input wave characterised by a significant height of $H_s = 2$ [m], and a peak period of $T_p = 6$ [s], *i.e.* a peak frequency of ≈ 1 [rad/s], consistent with the resonance frequency of the device (and the most energetic period of the Mediterranean sea - see [22]). Every performance analysis is computed in term of total absorbed mechanical power P_a for a given time interval $\Xi = [0,\, T_{sim}] \subset \mathbb{R}^+$ as

$$P_a = \frac{1}{T_{sim}} \int_{\Xi} u\lambda \mathrm{d}t = \frac{1}{T_{sim}} \int_{\Xi} P_i \mathrm{d}t, \tag{31}$$

where $P_i = u\lambda$ is the associated instantaneous mechanical power. A number of conclusions can be directly elucidated from Figure 15, which are discussed in the following [9]. At first glance, it is clear that the feedforward LiTe-Con controller (see Section 4.2.2) outperforms any other implemented strategy, with the feedback PI controller (see Section 4.1.2) following closely. This is, naturally, highly consistent with the quality of the approximating solutions in the neighborhood of the peak frequency characterising the wave input (see Figures 7 and 10). Specifically, the 'superiority' of the LiTe-Con solution sits on its broadband nature, being capable of approximate the optimality condition for a broad range $\mathcal{W}$, as opposed to interpolate at a single point in frequency. We can find the proportional (static) controller (see Section 4.1.1) ranking in 'last position', mostly since the structure of the corresponding feedback controller is merely a constant, and can only interpolate the magnitude of the optimal condition at the resonant frequency of the system.

Aiming at further analysing the most prominent solutions (in terms of

[9] Note that analogous conclusions can be made for any $T_p \in [3.5, 10.5]$.

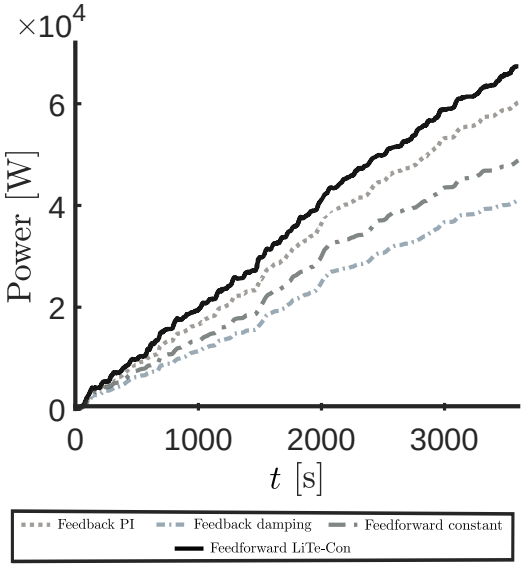

Figure 15: Power absorption results for the set of proposed controllers, for a wave input with $H_s = 2$ [m] and $T_p = 6$ [s].

energy-maximising performance), Figure 16 shows the time-domain output response of the PeWEC system (*i.e.* velocity λ of the controlled DoF) when a PI controller (solid-grey), and a LiTe-Con structure (dashed-green) are considered to control the device. Note that, though both controllers can consistently respect the corresponding physical limitations (see Table 3 and note that the maximum torque on the pendulum side is $T^{pen}_{max} = T_{max}\tau$, hence the maximum speed is $\omega^{pen}_{max} = \omega_{max}/\tau$), the LiTe-Con is able to exploit more effectively the operational space, resulting in a higher power absorption.

To further extend the power absorption analysis performed in Figure 15, Figure 17 illustrates performance results for the full set of peak periods characterising the wave resource in the Mediterranean sea. In particular, each controller performance are evaluated through power extraction and the so-

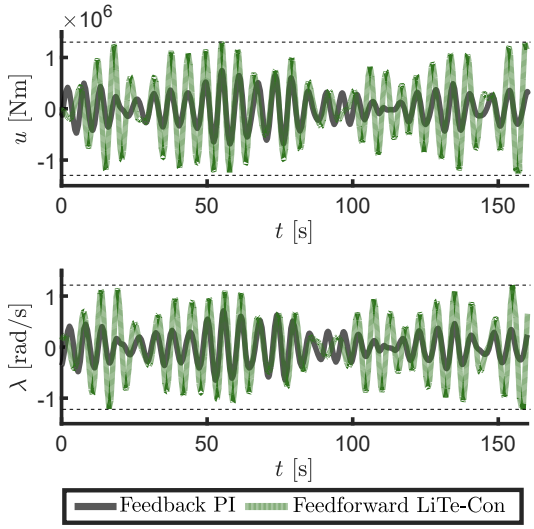

Figure 16: Time-traces obtained with the Feedback PI and the LiTe-Con controllers considering $Tp = 6s$. Note that for both applications the time-traces are within the constraint bounds.Note that u and λ are the control torque and the angular velocity of the PTO shaft respectively (see Section 2).

called relative capture width (RCW) of the device defined as:

$$\mathrm{RCW}_{\%} = \frac{P_a}{0,49 T_e H_s^2 W} \times 100, \tag{32}$$

where the denominator in 32 expresses the total wave input power affecting the PeWEC system over the width dimension W of the floater. We recall that both numerator and denominator of Equation 32 are expressed in [kW], for coherence. Consistently with those results presented in Figure 15, the LiTe-Con controller outperforms the set of synthesised controllers for virtually all peak wave periods, followed closely by the feedback PI strategy. The Lite-Con controller has a positive impact on the PeWEC power conversion efficiency, recording a $RCW_{\%}$ peak of about 25%. Finally, and to provide a comparison with a numerical-optimisation-based benchmark, Fig-

ure 18 shows the so-called relative generated power (RGP), computed, for each value of T_p, as

$$\text{RGP} = \frac{P^C}{P^B} \in [0, 1], \tag{33}$$

where P^C denotes the power absorbed by the particular controller being analysed, and P^B denotes the power absorbed by the benchmark controller. In this study, and motivated by the inherent presence of reactive PI controllers in the literature of WEC control, the benchmark controller is selected as defined in equation (23), with a set of coefficients $\{k_p, k_i\}$ *optimised for each specific wave condition*. In particular, we consider the (local) optimisation algorithm explored in [46, 43]. It can be readily appreciated that, once again, the LiTe-Con design remains relatively close to the benchmark condition for $T_p > 6$ [s], *i.e.* where the controller best approximates the optimal energy-maximising condition (see also Figure 12), followed closely by the feedback PI structure.

5.1. Critical comparison between controllers

A critical comparison can be elaborated from the results presented along both in Section 4 (design and synthesis), and Section 5 (performance analysis), in particular regarding the trade-off between simplicity and energy-maximising performance for the proposed controllers. We summarise such a comparison analysis via Table 4, proposing the following scoring system:

> *Simplicity*: Scale from 1 (red) to 4 (green), where 4 denotes the most simple strategy, in terms of design and implementation.
>
> *Performance*: Scale from 1 (red) to 4 (green), where 4 denotes the most efficient controller, in terms of overall energy absorption for the complete set of wave spectra characterising the Mediterranean sea.

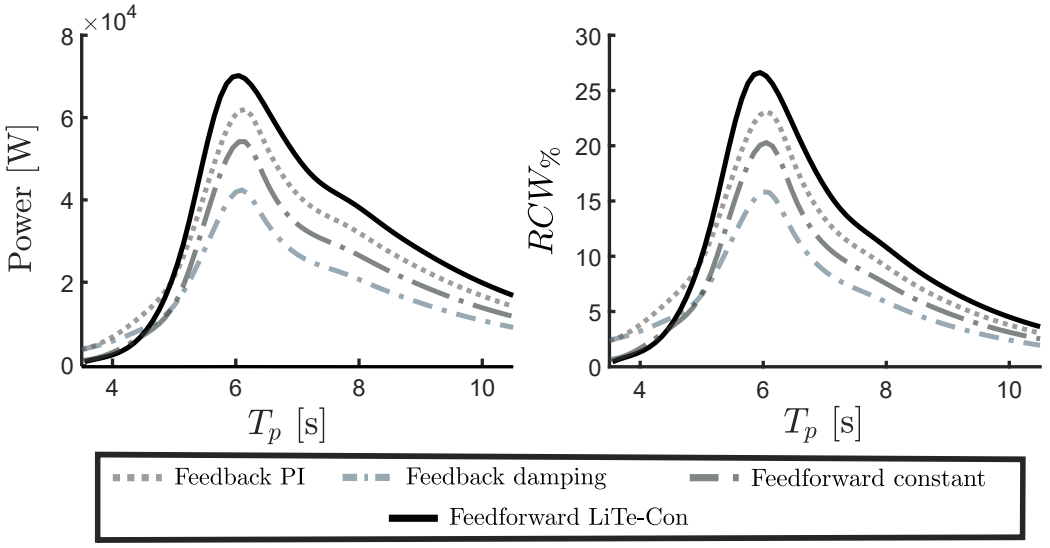

Figure 17: Power absorption (left) and $RCW_{\%}$ (right) results for the set of typical wave periods characterising the Mediterranean sea. The significant wave height is set to $H_w = 2$ [m].

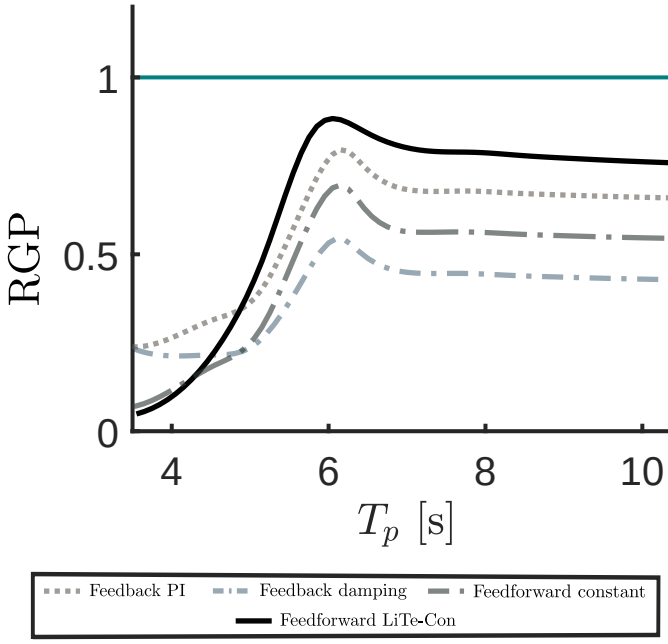

Figure 18: Relative generated power for the set of proposed controllers.

Table 4: Controller comparison. Feedback solutions are denoted with FF, while feedback controllers are denoted with FB.

Controller	**Type**	**Simplicity**	**Performance**
LiTe-Con controller	FF	1	4
PI controller	FB	3	3
Feedforward constant	FF	2	2
P controller	FB	4	1

A straightforward conclusion, arising directly from Table 4, is that simplicity and performance are, effectively, consistently conflicted: Controllers with better energy maximising performance, require more elaborated (and hence less simple) design/synthesis procedures. In particular, the LiTe-Con controller is that with best overall performance, and hence is rated with the highest mark (4). Nonetheless, its design is also rated as the least simple (4), since the overall structure requires tailored system identification procedures, potentially high-order representations for H_{ff}, and an estimate of the excitation force (*i.e.* requires a specific 'extra' structure to maximise energy absorption). The PI controller is that following in performance (3), with a relatively low degree of design complexity (though note that closed-loop stability is not necessarily guaranteed), hence earning a mark of (3) in simplicity. We reserve the highest simplicity ranking (4) for the proportional controller, since its design and synthesis is straightforward, both from an energy-maximising, and closed-loop stability perspectives. Continuing with Table 4, one can find the feedforward constant controller, which we rate with a (2) in simplicity, since, though also proportional as in the case of the feedback P controller, this specific structure requires in addition an estimate

of the total wave excitation force. Nonetheless, its overall performance in terms of power absorption is rated with a (2), taking the third position in the table. Finally, though very simple to design and implement, we rate the performance of the proportional feedback controller with the lowest mark (1), since its associated power absorption is consistently lower than those related to the remaining controllers.

6. Conclusions

We propose, in this paper, a set of four simple and intuitive controllers to maximise energy absorption for the multi-DoF underactuated PeWEC wave energy converter. To pursuit this objective, we derive the (non-causal) IM energy-maximising conditions for PeWEC, and propose different fully LTI structures to approximate the corresponding non-implementable optimality conditions. Given their LTI nature, the controllers proposed in this manuscript are straightforward to design and implement, avoiding the requirement of computationally demanding optimisation routines to solve for a control solution. In addition to outline each corresponding design and synthesis procedure, we provide a performance analysis of the proposed controllers taking into account the wave resource in the location where PeWEC is designed to operate. A critical comparison of the controllers is also provided not only in terms of power absorption, but also in terms of design/synthesis simplicity.

Acknowledgments

This project has received funding from the European Union's Horizon 2020 research and innovation programme under the Marie Sklodowska-Curie grant

agreement No 101024372. The results of this publication reflect only the author's view and the European Commission is not responsible for any use that may be made of the information it contains.

References

[1] Babarit, A., Delhommeau, G., 2015. Theoretical and numerical aspects of the open source BEM solver NEMOH, in: 11th European Wave and Tidal Energy Conference (EWTEC2015), Nantes, France. URL: https://hal.archives-ouvertes.fr/hal-01198800.

[2] Bacelli, G., Nevarez, V., G. Coe, R., G. Wilson, D., 2020. Feedback Resonating Control for a Wave Energy Converter. IEEE Transactions on Industry Applications 56, 1862–1868. doi:10.1109/TIA.2019.2958018.

[3] Bracco, G., Cagninei, A., Giorcelli, E., Mattiazzo, G., Poggi, D., Raffero, M., 2016. Experimental validation of the ISWEC wave to PTO model. Ocean Engineering 120. doi:10.1016/j.oceaneng.2016.05.006.

[4] Carapellese, F., Sirigu, S.A., Bonfanti, M., Mattiazzo, G., 2021. Multiobjective optimisation approaches applied to a wave energy converter design, in: Proceedings of the European Wave and Tidal Energy Conference.

[5] Cummins, W., Iiuhl, W., Uinm, A., 1962. The impulse response function and ship motions .

[6] Faedo, N., 2020. Optimal control and model reduction for wave energy systems: A moment-based approach.

[7] Faedo, N., Bussi, U., Peña-Sanchez, Y., Windt, C., Ringwood, J.V., 2021a. A simple and effective excitation force estimator for wave energy systems. IEEE PES Transaction on Sustainable Energy .

[8] Faedo, N., Carapellese, F., Pasta, E., Mattiazzo, G., 2021b. On the principle of impedance-matching for underactuated wave energy harvesting system. Applied Ocean Research .

[9] Faedo, N., Olaya, S., Ringwood, J.V., 2017. Optimal control, MPC and MPC-like algorithms for wave energy systems: An overview. IFAC Journal of Systems and Control 1, 37–56. doi:10.1016/j.ifacsc.2017.07.001.

[10] Faedo, N., Peña-Sanchez, Y., Ringwood, J.V., 2018. Finite-order hydrodynamic model determination for wave energy applications using moment-matching. Ocean Engineering 163, 251–263. doi:10.1016/j.oceaneng.2018.05.037.

[11] Falnes, J., 2002. Ocean Waves and Oscillating Systems. Cambridge University Press. doi:10.1017/CBO9780511754630.

[12] Fusco, F., Ringwood, J.V., 2013. A simple and effective real-time controller for wave energy converters. IEEE Transactions on Sustainable Energy 4, 21–30.

[13] García-Violini, D., Faedo, N., Jaramillo-Lopez, F., Ringwood, J.V., 2020. Simple Controllers for Wave Energy Devices Compared. Journal of Marine Science and Engineering 8, 793. doi:10.3390/jmse8100793.

[14] Garcia-Violini, D., Pena-Sanchez, Y., Faedo, N., Ringwood, J.V., 2020. An Energy-Maximising Linear Time Invariant Controller (LiTe-Con) for

Wave Energy Devices. IEEE Transactions on Sustainable Energy 11, 2713–2721. doi:10.1109/TSTE.2020.2971392.

[15] Gaspar, J.F., Calvário, M., Kamarlouei, M., Guedes Soares, C., 2016. Power take-off concept for wave energy converters based on oil-hydraulic transformer units. Renewable Energy 86, 1232–1246. doi:10.1016/j.renene.2015.09.035.

[16] Genta, G., 2009. Vibration Dynamics and Control. Mechanical Engineering Series, Springer US, Boston, MA. doi:10.1007/978-0-387-79580-5.

[17] Giorgi, G., Sirigu, S., Bonfanti, M., Bracco, G., Mattiazzo, G., 2021. Fast nonlinear Froude–Krylov force calculation for prismatic floating platforms: a wave energy conversion application case. Journal of Ocean Engineering and Marine Energy 7, 439–457. doi:10.1007/s40722-021-00212-z.

[18] Goodwin, G., Graebe, S., Salgado, M.E., 2001. Control system design. Upper Saddle River, NJ: Prentice Hall.

[19] Gunn, K., Stock-Williams, C., 2012. Quantifying the global wave power resource. Renewable Energy 44, 296–304. doi:10.1016/j.renene.2012.01.101.

[20] Hasselmann, K., Barnett, T., Bouws, E., Carlson, H., Cartwright, D.E., Eake, K., Euring, J., Gicnapp, A., Hasselmann, D., Kruseman, P., 1973. Measurements of wind-wave growth and swell decay during the joint

north sea wave project (jonswap). Ergaenzungsheft zur Deutschen Hydrographischen Zeitschrift, Reihe A .

[21] Korde, U., Ringwood, J., 2016. Hydrodynamic control of wave energy devices. Cambridge University press.

[22] Liberti, L., Carillo, A., Sannino, G., 2013. Wave energy resource assessment in the Mediterranean, the Italian perspective. Renewable Energy 50. doi:10.1016/j.renene.2012.08.023.

[23] Liberzon, D., 2011. Calculus of variations and optimal control theory. Princeton university press.

[24] Ljung, L., 1998. System identification, in: Signal analysis and prediction. Springer.

[25] Mattiazzo, G., 2019. State of the Art and Perspectives of Wave Energy in the Mediterranean Sea: Backstage of ISWEC. Frontiers in Energy Research 7. doi:10.3389/fenrg.2019.00114.

[26] Merigaud, A., Ringwood, J.V., 2018. Free-Surface Time-Series Generation for Wave Energy Applications. IEEE Journal of Oceanic Engineering 43, 19–35. doi:10.1109/JOE.2017.2691199.

[27] Paduano, B., Giorgi, G., Gomes, R.P.F., Pasta, E., Henriques, J.C.C., Gato, L.M.C., Mattiazzo, G., 2020. Experimental Validation and Comparison of Numerical Models for the Mooring System of a Floating Wave Energy Converter. Journal of Marine Science and Engineering 8. doi:10.3390/jmse8080565.

[28] Paduano, B., Pasta, E., Papini, G., Carapellese, F., Bracco, G., 2021. Mooring influence on the productivity of a pitching wave energy converter, in: OCEANS 2021: San Diego – Porto, pp. 1–6. doi:10.23919/OCEANS44145.2021.9706108.

[29] Pasta, E., Carapellese, F., Mattiazzo, G., 2021. Deep Neural Network Trained to Mimic Nonlinear Economic ModelPredictive Control: an Application to a Pendulum Wave EnergyConverter, in: IEEE CSS Conference on Control Technology and Applications.

[30] Pena-Sanchez, Y., Faedo, N., Penalba, M., Giuseppe, G., Mérigaud, A., Windt, C., Violini, D., LiGuo, W., Ringwood, J., 2019. Finite-Order hydrodynamic Approximation byMoment-Matching (FOAMM) toolbox for waveenergy applications, in: 13th European Wave and Tidal Energy Conference (EWTEC).

[31] Pena-Sanchez, Y., Windt, C., Davidson, J., Ringwood, J.V., 2020. A Critical Comparison of Excitation Force Estimators for Wave-Energy Devices. IEEE Transactions on Control Systems Technology 28, 2263–2275. doi:10.1109/TCST.2019.2939092.

[32] Penalba, M., Kelly, T., Ringwood, J., 2017. Using nemoh for modelling wave energy converters: A comparative study with wamit, in: 12th European Wave and Tidal Energy Conference (EWTEC).

[33] Perez, T., Fossen, T.I., 2008. Time- vs. Frequency-domain Identification of Parametric Radiation Force Models for Marine Structures at Zero

Speed. Modeling, Identification and Control: A Norwegian Research Bulletin 29, 1–19. doi:10.4173/mic.2008.1.1.

[34] Pozzi, N., Bracco, G., Passione, B., Sirigu, S.A., Mattiazzo, G., 2018. PeWEC: Experimental validation of wave to PTO numerical model. Ocean Engineering 167, 114–129. doi:10.1016/j.oceaneng.2018.08.028.

[35] Pozzi, N., Bracco, G., Passione, B., Sirigu, S.A., Vissio, G., Mattiazzo, G., Sannino, G., 2017. Wave Tank Testing of a Pendulum Wave Energy Converter 1:12 Scale Model. International Journal of Applied Mechanics 09. doi:10.1142/S1758825117500247.

[36] Raffero, M., Martini, M., Passione, B., Mattiazzo, G., Giorcelli, E., Bracco, G., 2015. Stochastic Control of Inertial Sea Wave Energy Converter. The Scientific World Journal 2015, 1–14. doi:10.1155/2015/980613.

[37] Rafiee, A., Fiévez, J., 2015. Numerical prediction of extreme loads on the ceto wave energy converter.

[38] Ringwood, John V.; Bacelli, Giorgio; Fusco, F., 2014. Energy-Maximizing Control of Wave-Energy Converters: The Development of Control System Technology to Optimize Their Operation. IEEE Control Systems 34, 30–55. doi:10.1109/MCS.2014.2333253.

[39] Salter, S.H., 1974. Wave power. Nature 249, 720–724. doi:10.1038/249720a0.

[40] Salter, S.H., Taylor, J.R.M., Caldwell, N.J., 2002. Power conversion

mechanisms for wave energy. Proceedings of the Institution of Mechanical Engineers, Part M: Journal of Engineering for the Maritime Environment 216, 1–27. doi:10.1243/147509002320382103.

[41] Scruggs, J., Lattanzio, S., Taflanidis, A., Cassidy, I., 2013. Optimal causal control of a wave energy converter in a random sea. Applied Ocean Research 42, 1–15. doi:10.1016/j.apor.2013.03.004.

[42] Sergiienko, N.Y., Cocho, M., Cazzolato, B.S., Pichard, A., 2021. Effect of a model predictive control on the design of a power take-off system for wave energy converters. Applied Ocean Research 115, 102836. doi:10.1016/j.apor.2021.102836.

[43] Silva, L., Sergiienko, N., Pesce, C., Ding, B., Cazzolato, B., Morishita, H., 2020. Stochastic analysis of nonlinear wave energy converters via statistical linearization. Applied Ocean Research 95, 102023. doi:10.1016/j.apor.2019.102023.

[44] Sirigu, S.A., Bonfanti, M., Begovic, E., Bertorello, C., Dafnakis, P., Giorgi, G., Bracco, G., Mattiazzo, G., 2020a. Experimental Investigation of the Mooring System of a Wave Energy Converter in Operating and Extreme Wave Conditions. Journal of Marine Science and Engineering 8, 180. doi:10.3390/jmse8030180.

[45] Sirigu, S.A., Foglietta, L., Giorgi, G., Bonfanti, M., Cervelli, G., Bracco, G., Mattiazzo, G., 2020b. Techno-Economic Optimisation for a Wave Energy Converter via Genetic Algorithm. Journal of Marine Science and Engineering 8, 482. doi:10.3390/jmse8070482.

[46] Sirigu, S.A., Vissio, G., Bracco, G., Giorcelli, E., Passione, B., Raffero, M., Mattiazzo, G., 2016. ISWEC design tool. International Journal of Marine Energy 15, 201–213. doi:10.1016/j.ijome.2016.04.011.

[47] Song, J., Abdelkhalik, O., Robinett, R., Bacelli, G., Wilson, D., Korde, U., 2016. Multi-resonant feedback control of heave wave energy converters. Ocean Engineering 127, 269–278. doi:10.1016/j.oceaneng.2016.09.046.

[48] Taghipour, R., Perez, T., Moan, T., 2008. Hybrid frequency–time domain models for dynamic response analysis of marine structures. Ocean Engineering 35, 685–705. doi:10.1016/j.oceaneng.2007.11.002.

[49] Todalshaug, J.H., Ásgeirsson, G.S., Hjálmarsson, E., Maillet, J., Möller, P., Pires, P., Guérinel, M., Lopes, M., 2016. Tank testing of an inherently phase-controlled wave energy converter. International Journal of Marine Energy 15. doi:10.1016/j.ijome.2016.04.007.

[50] Vidyasagar, M., 2002. Nonlinear systems analysis. SIAM.

[51] Von Stryk, O., 1993. Numerical solution of optimal control problems by direct collocation, in: Optimal control. Springer.